3526 *Chem. Mater.* **2009,** *21,* 3526–3535
DOI:10.1021/cm803290b

CHEMISTRY OF MATERIALS
Article

Preparation of Stable Water-Dispersible PEGylated Gold Nanoparticles Assisted by Nonequilibrium Atmospheric-Pressure Plasma Jets

Hitoshi Furusho,[†] Katsuhisa Kitano,[‡,⊥] Satoshi Hamaguchi,[‡,⊥] and Yukio Nagasaki*[,†,§,⊥,¶,□]

[†]*Institute of Materials Science, Graduate School of Pure and Applied Science,* [§]*Tsukuba Research Center for Interdisciplinary Materials Science,* [⊥]*Center for Tsukuba Advanced Research Alliance,* [¶]*Master's School of Medical Sciences, Graduate School of Comprehensive Human Sciences,* [□]*Satellite Laboratory of International Center for Materials Nanoarchitectonics, University of Tsukuba, Ten-noudai 1-1-1, Tsukuba, Ibaraki 305-8575, Japan, and* [‡]*Center for Atomic and Molecular Technologies, Graduate School of Engineering, Osaka University, Yamada-oka 2-1, Suita, Osaka 565-0871, Japan*

Received December 6, 2008. Revised Manuscript Received May 31, 2009

Water-dispersible gold nanoparticles with narrow size distributions were prepared by irradiation of nonequilibrium atmospheric-pressure dielectric-barrier-discharge (DBD) helium plasma jets to tetrachloroauric acid solutions containing poly(ethylene glycol) (PEG) that had a pentaethylenehexamine at one end of each polymer chain (N6-PEG). N6-PEG is known to interact with aurate cations to facilitate nucleation and growth of gold nanoparticles as a surface-modification agent. The helium-based DBD plasma jets contain energetic electrons and free radicals, which can induce chemical reactions on the surface of and/or in a solution at room temperature. For gold nanoparticles formed by DBD plasma-jet irradiation with the molar ratio of tetrachloroauric acid/N6-PEG being 1:20 at pH 10, the average particle size was in the range of 5−10 nm in diameter from transmission electron microscopy observation. Furthermore, gold nanoparticles prepared in this manner are found to have remarkable stability under physiological conditions because of the immobilization of PEG-derived materials on the gold surfaces. Such gold nanoparticles may therefore be considered excellent candidates for high-performance bionanoparticles.

1. Introduction

Metal nanoparticles have attracted considerable attention because of their versatile applications such as biomedical sensing devices[1−7] and electric devices.[8−11] Nanoparticles with diameters in the range of 1−100 nm have some specific properties arising from quantum size effects.[12−15] These properties are strongly dependent upon, for example, the shape,[13] size,[14] and coating materials of the nanoparticles[15] and dielectric constant of the dispersing media.[16−18]

In a solution containing gold nanoparticles, strong optical absorption occurs because of the surface-plasmon band of gold nanoparticles in the visible region at 520 nm in wavelength. The surface-plasmon band arises from collective oscillations of spreading electron clouds on the surfaces of a gold nanoparticle, which correlate with the electromagnetic field of the incoming light. This optical absorption gives the solution a distinguished color if the sizes of the gold nanoparticles are in the range of 5−120 nm in diameter.

The maximum absorption (λ_{max}) and the surface-plasmon bandwidth depend on the particle size, aggregation status, and dielectric constant of the solvent.[16−19] For

*Corresponding author. E-mail: yukio@nagalabo.jp.

(1) Mirkin, C. A.; Letsinger, R. L.; Mucic, R. C.; Storhoff, J. J. *Nature* **1996**, *382*, 607–609.
(2) Elghanian, R.; Storhoff, J. J.; Mucic, R. C.; Letsinger, R. L.; Mirkin, C. A. *Science* **1997**, *277*, 1078–1081.
(3) Alper, P. B.; Hendrix, M.; Sears, P.; Wong, C.-H. *J. Am. Chem. Soc.* **1998**, *120*, 1965–1978.
(4) Andrew Taton, T.; Mucic, R. C.; Mirkin, C. A.; Letsinger, R. L. *J. Am. Chem. Soc.* **2000**, *122*, 6305–6306.
(5) Niemeyer, C. M. *Angew. Chem., Int. Ed.* **2001**, *40*, 4128–4158.
(6) Otsuka, H.; Akiyama, Y.; Nagasaki, Y.; Kataoka, K. *J. Am. Chem. Soc.* **2001**, *123*, 8226–8230.
(7) Nagasaki, Y. *Chem. Lett.* **2008**, *37*(6), 564–569.
(8) Tanahashi, I.; Manabe, Y.; Tohda, T.; Sasaki, S.; Nakamura, A. *J. Appl. Phys.* **1996**, *79*, 1244–1249.
(9) Griffith Freeman, R.; Grabar, K. C.; Allison, K. J.; Bright, R. M.; Davis, J. A.; Guthrie, A. P.; Hommer, M. B.; Jackson, M. A.; Smith, P. C.; Walter, D. G.; Natan, M. J. *Science* **1995**, *267*, 1629–1632.
(10) Feldheim, D. L.; Grabar, K. C.; Natan, M. J.; Mallouk, T. E. *J. Am. Chem. Soc.* **1996**, *118*, 7640–7641.
(11) Andres, R. P.; Bein, T.; Dorogi, M.; Feng, S.; Henderson, J. I.; Kubiak, C. P.; Mahoney, W.; Osifchin, R. G.; Reifenberger, R. *Science* **1996**, *272*, 1323–1325.
(12) Alivisatos, A. P. *Science* **1996**, *271*, 933–937.
(13) Jin, R.; Cao, Y. W.; Mirkin, C. A.; Kelly, K. L.; Schatz, G. C.; Zheng, J. G. *Science* **2001**, *294*, 1901–1903.
(14) Rotello, V. Nanoparticles Building Blocks for Nanotechnology; Kluwer Academic Nanoparticle: New York, 2004; pp 173−200.
(15) Aiken, J. D.III; Finke, R. G. *J. Mol. Catal. A: Chem.* **1999**, *145*, 1–44.
(16) Mulvaney, P. *Langmuir* **1996**, *12*, 788–800.
(17) Nath, N.; Chilkoti, A. *Anal. Chem.* **2004**, *76*, 5370–5378.
(18) Cheng, S.-F.; Chau, L.-K. *Anal. Chem.* **2003**, *75*, 16–21.
(19) Daniel, M.-C.; Astruc, D. *Chem. Rev.* **2004**, *104*, 293–346.

Published on Web 07/17/2009

example, aggregation of gold nanoparticles shifts the absorption peak toward a longer wavelength and accordingly changes the color of the colloidal solution from deep red to purple. Recently, such characteristics have been used for various bioanalyses, such as DNA diagnosis by hybridization of gold nanoparticles having single-chain DNAs with their cDNAs,[20−24] molecular recognition by sugar-lectin bonding,[25,26] and biotin−avidin protein interactions.[27−30] These analytical techniques are based on aggregation or cross-linking between target molecules and surface-modified gold nanoparticles.

Gold nanoparticles for biological applications have been prepared with the use of various kinds of reducing agents, such as citric acid,[31] sodium borohydride,[32] and ascorbic acid.[33] For example, in 1994, Brust and Schiffrin reported the synthesis of thiol-modified gold nanoparticles using a two-phase liquid−liquid system.[34,35] It is the first size-controlled synthesis that produced gold nanoparticles with dispersion stability in organic solvents. The thiol-capped gold nanoparticles synthesized in this method can be repeatedly isolated and redissolved in common organic solvents without aggregation or decomposition.

For biomedical applications, however, colloid stability under physiological conditions (e.g., for human blood, pH 7.4 and salt concentration of 150 mM) is an essential factor. In general, in the absence of a repulsive force against the van der Waals attractive interaction, metal colloids tend to aggregate. Therefore, the use of a stabilizer that induces such repulsive forces is necessary to ensure the stability of nanoparticles in various media. Electrostatic and steric stabilization methods are commonly used. However, electrostatic stabilization is affected by the ionic strength of a nanoparticle, which varies with the thickness of the electron double layer around the nanoparticle in a solvent. Steric stabilization is therefore more suitable for biomedical applications. For example, poly(ethylene glycol) (PEG) that has a specific ligand group at one end of each polymer chain is a preferred stabilizer for metal nanoparticles in aqueous media.[25,36−39] The stabilization of metal colloids has been achieved by the coordination of several ligands, such as phosphines, amines, and thiols, on the surfaces of metal nanoparticles. One of the other issues of metal colloid for biomedical application is contamination from a reducing agent. As stated above, certain reducing agents must be utilized for preparation of the metal colloid.[40,41] We have to completely remove such contaminants from the system.

We previously reported a method of preparation for dispersion-stable gold nanoparticles using PEG-*block*-poly[2-(*N*,*N*-dimethylamino)ethyl methacrylate] (PEG-*b*-PAMA) with an α-biotinyl group at one end of each PEG chain in aqueous solutions.[30,42,43] We found that PEG-*b*-PAMA acted not only as a particle stabilizer but also as a reducing agent. Indeed, PEGylated gold nanoparticles with highly stable dispersion under physiological conditions were obtained by simply mixing PEG-*b*-PAMA with tetrachloroauric acid in aqueous solutions. It was the first report on the in situ preparation of dispersion-stable gold nanoparticles based only on the reduction properties of amines without a common reductant. Coordination of the nitrogen of PEG-*b*-PAMA with the surface of a gold nanoparticle is an essential factor for stable water dispersion. The most suitable number of PAMA units in the block copolymer has been found recently to range from 3 to 6.[44]

Recently, two of the authors (K.K. and S.H.) have developed a portable dielectric-barrier-discharge (DBD) plasma-jet system that operates with helium gas at atmospheric pressure.[45] As shown in Figure 1, plasma jets are emitted from a dielectric tube (that may be made of, e.g., glass, quartz, or plastic), around which a powered electrode is wound. A helium gas flows in the dielectric tube. In this system, a high voltage of approximately 10 kV in peak value is applied to the electrode with a frequency of 10 kHz. The plasma may be called a DBD plasma because the discharge is generated inside the dielectric tube, which prevents the conduction current from flowing into the discharge from the powered electrode; i.e., the tube acts as a dielectric barrier. It is also called "jet" because the

(20) Storhoff, J. J.; Elghanian, R.; Mucic, R. C.; Mirkin, C. A.; Letsinger, R. L. *J. Am. Chem. Soc.* **1998**, *120*, 1959–1964.
(21) Mucic, R. C.; Storhoff, J. J.; Mirkin, C. A.; Letsinger, R. L. *J. Am. Chem. Soc.* **1998**, *120*, 12674–12675.
(22) Loweth, C. J.; Caldwell, W. B.; Peng, X.; Alivisators, A. P.; Schultz, P. G. *Angew. Chem., Int. Ed.* **1999**, *38*, 1808–1812.
(23) Sato, K.; Hosokawa, K.; Maeda, M. *J. Am. Chem. Soc.* **2003**, *125*, 8102–8103.
(24) Sato, K.; Onoguchi, M.; Sato, Y.; Hosokawa, K.; Maeda, M. *Anal. Biochem.* **2006**, *350*, 162–164.
(25) Otsuka, H.; Akiyama, Y.; Nagasaki, Y.; Kataoka, K. *J. Am. Chem. Soc.* **2001**, *123*, 8226–8230.
(26) Takae, S.; Akiyama, Y.; Yamasaki, Y.; Nagasaki, Y.; Kataoka, K. *Bioconjugate Chem.* **2007**, *18*, 1241–1245.
(27) Gestwicki, J. E.; Cairo, C. W.; Strong, L. E.; Oetjen, K. A.; Kiessling, L. L. *J. Am. Chem. Soc.* **2002**, *124*, 14922–14933.
(28) Mann, D. A.; Kanai, M.; Maly, D. J.; Kiessling, L. L. *J. Am. Chem. Soc.* **1998**, *120*, 10575–10582.
(29) Kingery-Wood, J. E.; Williams, K. W.; Sigal, G. B.; Whitesides, G. M. *J. Am. Chem. Soc.* **1992**, *114*, 7303–7305.
(30) Nagasaki, Y.; Ishii, T.; Sunaga, Y.; Watanabe, Y.; Otsuka, H.; Kataoka, K. *Langmuir* **2004**, *20*, 6396–6400.
(31) Brown, K. R.; Walter, D. G.; Natan, M. J. *Chem. Mater.* **2000**, *12*, 306–313.
(32) Wang, S.; Sato, S.; Kimura, K. *Chem. Mater.* **2003**, *15*, 2445–2448.
(33) Miranda, O. R.; Dollahon, N. R.; Ahmadi, T. S. *Cryst. Growth Des.* **2006**, *6*, 2747–2753.
(34) Brust, M.; Walker, M.; Bethell, D.; Schiffrin, D. J.; Whyman, R. *J. Chem. Soc., Chem. Commun.* **1994**, 801–802.
(35) Brust, M.; Fink, J.; Bethell, D.; Schiffrin, D. J.; Kiely, C. *J. Chem. Soc., Chem. Commun.* **1995**, 1655–1656.
(36) Takae, S.; Akiyama, Y.; Otsuka, H.; Nakamura, T.; Nagasaki, Y.; Kataoka, K. *Biomacromolecules* **2005**, *6*, 818–824.
(37) Foos, E. E.; Snow, A. W.; Twigg, M. E.; Ancona, M. G. *Chem. Mater.* **2002**, *14*, 2401–2408.
(38) Kanaras, A. G.; Kamounah, F. S.; Schaumburg, K.; Kiely, C. J.; Brust, M. *Chem. Commun.* **2002**, 2294–2295.
(39) Wuelfing, W. P.; Gross, S. M.; Miles, D. T.; Murray, R. W. *J. Am. Chem. Soc.* **1998**, *120*, 12696–12697.
(40) Awaleh, M. O.; Baril-Robert, F.; Reber, C.; Badia, A.; Brisse, F. *Inorg. Chem.* **2008**, *47*, 2964–2974.
(41) Foos, E. E.; Snow, A. W.; Twigg, M. E.; Ancona, M. G. *Chem. Mater.* **2002**, *14*, 2401–2408.
(42) Ishii, T.; Otsuka, H.; Kataoka, K.; Nagasaki, Y. *Langmuir* **2004**, *20*, 561–564.
(43) Ishii, T.; Sunaga, Y.; Otsuka, H.; Nagasaki, Y.; Kataoka, K. *J. Photopolym. Sci. Technol.* **2004**, *17*, 95–98.
(44) Miyamoto, D.; Oishi, M.; Kojima, K.; Yoshimoto, K.; Nagasaki, Y. *Langmuir* **2008**, *24*, 5010–5017.
(45) Aoki, H.; Kitano, K.; Hamaguchi, S. *Plasma Sources Technol.* **2008**, *17*(2), 025006/1–025006/6.

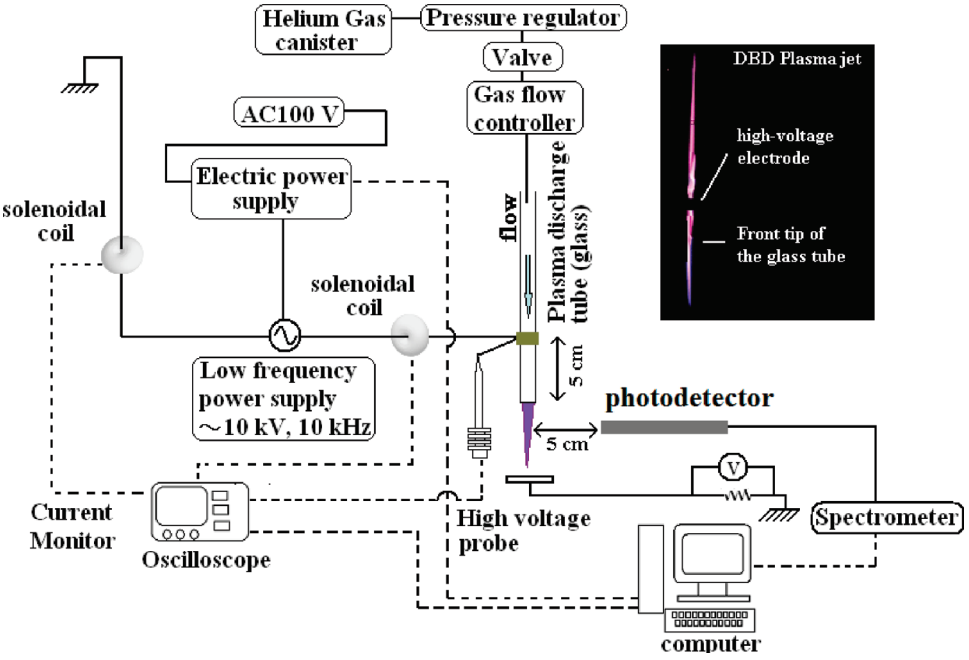

Figure 1. Schematic diagram of a DBD plasma-jet system and photograph of a DBD plasma jet (on the right in the dark background). The system is placed in ambient air. A helium gas flows in the glass tube, the inner and outer diameters of which are 3 and 6 mm. The high-voltage electrode is wound around the exterior of the glass tube. The distance between the lower edge of the electrode and the front tip of the glass tube is 5 cm. DBD plasma jets are emitted from the front tip of the glass tube to a material or a solution in a container placed on the grounded surface. For OES, a photodetector is placed level with the front tip of the glass tube. The distance between the photodetector and the plasma jets is 5 cm.

plasma typically seems emitted from the tip of the discharge tube. The gas temperature of the DBD plasma jet is close to room temperature, i.e., significantly lower than its electron temperature. In this sense, the DBD plasma jets are not in thermal equilibrium and therefore may be called nonequilibrium atmospheric-pressure plasma jets.

In such plasmas, highly reactive species such as nitrogen and hydroxyl radicals are present and can cause various chemical reactions. Indeed, as we shall discuss in the following sections, we have found that DBD plasma-jet irradiation to auric acid solutions can easily reduce aurate cations without any additional reducing agent, generating flakes of gold on the surface of the solution.

In the present paper, we describe methods of preparation for gold nanoparticles using DBD plasma jets generated in the system shown in Figure 1. The strategy that we have employed here is to use DBD plasma jets for the direct reduction of aurate cations without damaging complex formation between the amine ligands and aurate cations. Extremely rapid formation of nanoparticles with narrow size distributions and highly stable dispersion properties in aqueous media was observed when DBD plasma jets were irradiated to a mixed solution of tetrachloroauric acid and N6-PEG. The sizes of obtained gold nanoparticle were 5−10 nm, which was confirmed from high-resolution transmission electron microscopy (HRTEM). The PEG moieties were detected by pyrolysis gas chromatography−mass spectroscopy (GC−MS) of the purified gold nanoparticles, by which we confirmed the presence of PEG chains on the surfaces of gold nanoparticles.

2. Experimental Section

In the experiments presented here, we used commercial methoxy-ended PEG (number-average molecular weight, i.e., M_n = 2000; Aldrich), 4-(dimethylamino)pyridine (Tokyo Kasei), triethylamine (Tokyo Kasei), *p*-toluenesulfonyl chloride (Wako), ethylene chloride (Junsei Chemical), tetrachloroauric acid (Junsei Chemical), and pentaethylenehexamine (Tokyo Kasei) as received.

For analyses, size-exclusion chromatography (SEC) measurements were carried out using a TOSO HPLC-8120 gel permeation chromatograph equipped with TOSO gel permeation columns (TSK-GPC Super HZ4000 and TSK-GPC Super HZ3000). Tetrahydrofuran (THF) that contained triethylamine (1 wt %) was used as the eluent at a flow rate of 0.35 mL/min at 40 °C. The molecular masses of polymers were determined by matrix-assisted laser desorption/ionization time-of-flight mass spectrometer (MALDI-TOF MS; Applied Biosystems). The proton nuclear magnetic resonance (^{1}H NMR) spectra were obtained using chloroform-*d* solutions (containing tetramethylsilane at 0.1 wt %) with a JEOL EX300 spectrometer at 300 MHz. The sizes and shapes of the obtained nanoparticles were measured by TEM (Hitachi H-8000) and a dynamic light-scattering (DLS) spectrometer (Zeta-seizer Nano ZS, SEN3600) equipped with a 633 nm He−Ne laser and using a 1.5 mL cell. The surface-plasmon band was measured in a UV−visible spectrometer (UV-2550; Shimadzu). Optical emission spectroscopy (OES) for DBD plasma jets was performed with a spectrometer (Photal MCPD-7000; Otsuka Electronics Ltd.).

2-1. Synthesis of Pentaethylenehexamine-Ended PEG (N6-PEG). N6-PEG was synthesized according to the procedure shown in the Figure S1 of the Supporting Information.

2-1-1. Tosylation of MeO-PEG-OH. MeO-PEG-OH (M_n = 2000, 40 g, 20 mmol), *p*-toluenesulfonyl chloride (7.6 g, 40 mmol), and triethylamine (6.8 mL, 52 mmol) were dissolved in 500 mL of ethylene chloride in a round-bottomed flask. After

30 min of magnetic stirring, 4-(dimethylamino)pyridine (1.0 g, 8.2 mmol) was added to the reaction flask and stirred for an additional 24 h at room temperature. After the liberated salt was separated by filtration, the reaction mixture was poured into excess ether to precipitate the products. The obtained precipitate was dissolved in ethylene chloride and reprecipitated with ether. After filtration, the obtained tosylated PEG was dissolved in benzene and subjected to freeze-drying (yield = 94%; tosylation functionality = 99%). The ^{1}H NMR spectrum is shown in Figure S2a of the Supporting Information.

2-1-2. Synthesis of N6-PEG. The solution of tosylated PEG (2.0 g) in ethylene chloride (100 mL) was added dropwise to an ethylene chloride solution (50 mL) of pentaethylenehexamine (23.2 g, 100 mmol) and stirred for 7 days at room temperature. After the liberated salts were separated by filtration, the reaction mixture was poured into excess ether to precipitate the products. The obtained polymer was purified by dialysis (Cellulose Ester membrane, molecular weight cutoff [MWCO] of 1000; Spectrum Laboratories Inc.). The obtained polymer was then dissolved in benzene and subjected to freeze-drying.

The molecular mass of N6-PEG was determined by SEC using THF as the eluent. PEG standard samples were utilized to calculate the molecular mass. The SEC data of the obtained N6-PEG is shown in Figure S3a of the Supporting Information (M_n = 2240, M_w = 2170, and M_w/M_n = 1.03). MALDI-TOF MS was used to confirm the molecular mass of aminated PEG (see Figure S3b of the Supporting Information). The peak top of the mass fragment of N6-PEG was observed at 2210 (m/z). The SEC data of the obtained N6-PEG were almost coincident with those of MALDI-TOF MS.

The amination functionality was determined from the ^{1}H NMR (see Figure S2b of the Supporting Information) spectrum as the ratio of methylene protons adjacent to nitrogen to methylene protons adjacent to oxygen in the PEG segment, based on the molecular mass of PEG determined by SEC (yield = 35%; amination functionality = 40%). Dilute aqueous HCl (pH 3.0) was added to the obtained crude N6-PEG, and the polymer was purified by cation-exchange chromatography. After purification, the yield was 15%, and the amination functionality was 99%.

2-2. Synthesis of Gold Nanoparticles with DBD Plasma Jets. *2-2-1. DBD Plasma Jets*. A schematic illustration of the DBD plasma-jet discharge and measurement system is shown in Figure 1. A glass tube (inner diameter, 3.0 mm; outer diameter, 6 mm) was used as the plasma-discharge dielectric tube. A copper film with electrically conductive adhesive tape was attached to the exterior of the glass tube to form the high-voltage electrode. The purity of the helium gas used in the experiments presented here was 99.999%. The plasma used in the present study was generated by the application of 8 kV and 10 kHz voltage pulses to the electrode with a helium gas flowing at a rate of 10−90 L/min. The power supply system was LHV-13AC (LOGY Electric Co., Ltd.), and the helium gas flow was controlled by a gas flowmeter (model 3660 Series; Kofloc). OES was used for characterization of the plasmas.

2-2-2. Preparation of Gold Nanoparticles by Plasma-Induced Reduction in the Presence of N6-PEG. Gold nanoparticles were prepared by plasma-induced reduction of aurate cations (0.1 mM tetrachloroauric acid; pH 3.9 and 10 solutions) with N6-PEG (1 mM; pH 3.9 and pH 10 solutions) at tetrachloroauric acid/N6-PEG molar ratios of 1:5 to 1:20.

To prevent localized reactions caused by DBD plasma-jet irradiation, an ultrasonic cleaner was used as an agitator. It has been confirmed that no reduction of tetrachloroauric acid occurs with the use of the conventional ultrasonic apparatus (US-3R 120 W, 40 kHz, 5.9 L bath volume) only. Especially hot bubbles to cause pyrolysis of water are not produced at a detectable level in the ultrasonic apparatus used here.[46] Tetrachloroauric acid (0.1 mM, pH 3.9) was mixed with N6-PEG (1.0 mM, pH 3.9) at a molar ratio of 1:5. The pH levels were adjusted by the addition of a HCl or NaOH solution. The mixture of tetrachloroauric acid and N6-PEG was stirred by a magnetic stirrer for 60 s in ambient air, and DBD plasma jets were applied to the surface of the chilled solution in ambient air under ultrasonication. After the reaction, the N6-PEG-modified gold nanoparticles were precipitated by centrifugation at $10^5 g$ for 20 min at 4 °C. After the supernatant fluid was removed, the precipitate was resuspended in a buffer of the same pH. This process was repeated three times to produce pure N6-PEG-modified gold nanoparticles.

2-2-3. Preparation of Gold Nanoparticles with N6-PEG without Using the DBD Plasma Jet. As a control for plasma-induced reduction, gold nanoparticles were prepared using N6-PEG only. For this purpose, 0.1 mM tetrachloroauric acid (pH 3.9) was mixed with a 1 mM N6-PEG solution (pH 3.9) at a molar ratio of 1:5. After 48 h of magnetic stirring of the solution exposed to ambient air, the generated N6-PEG-modified gold nanoparticles were precipitated by centrifugation at $10^5 g$ for 20 min at 4 °C. After the supernatant fluid was removed, the precipitate was resuspended in a buffer of the same pH. This process was repeated three times to produce pure N6-PEG-modified gold nanoparticles.

3. Results and Discussion

3-1. Characteristics of DBD Plasma jets. OES for helium DBD plasma jets (where the applied peak voltage was 8 kV, the frequency was 10 kHz, and the helium gas flow rate was 60 L/min) was performed in the wavelength region from 200 to 800 nm. Figure 2 shows emission spectra from DBD plasma jets emitted into (a) ambient air, (b) a quartz cell, and (c) a quartz cell that contains water. Here some spectral lines are identified as indicated. Although the operating gas for the discharge is helium, emission lines of hydroxyls and nitrogen-derived species such as NH, N_2, and N_2^+ are also present because of humidity, oxygen, and nitrogen in the ambient air.[47,48] As shown in Figure 2b, when the plasma jets are injected into a quartz cell, strong emission lines of helium excited species are observed in addition to those from hydroxyl radicals because the quartz cell (4.5 mL) is mostly filled with helium. In part (b), on the other hand, emission lines of nitrogen-derived species are practically undetectable. When 1 mL of water is put into the quartz cell (4.5 mL), the intensities of all emission lines decrease significantly, as shown in Figure 2c, which may be caused by quenching or dissolution of excited species when they are in contact with water.

(46) Okitsu, K.; Yue, A.; Tanabe, S.; Matsumoto, H.; Yobiko, Y. *Langmuir* **2001**, *17*, 7717–7720.
(47) Kurniawan, K. H.; Pardede, M.; Hedwig, R.; Lie, Z. S.; Lie, T. J.; Kurniawan, D. P.; Ramli, M.; Fukumoto, K.-i.; Niki, H.; Abdulmadjid, S. N.; Idris, N.; Maruyama, T.; Kagawa, K.; Tjia, M. O. *Anal Chem*. **2007**, *79*, 2703–2707.
(48) Jin, Z.; Su, Y.; Duan, Y. *Anal. Chem*. **2001**, *73*, 360–365.

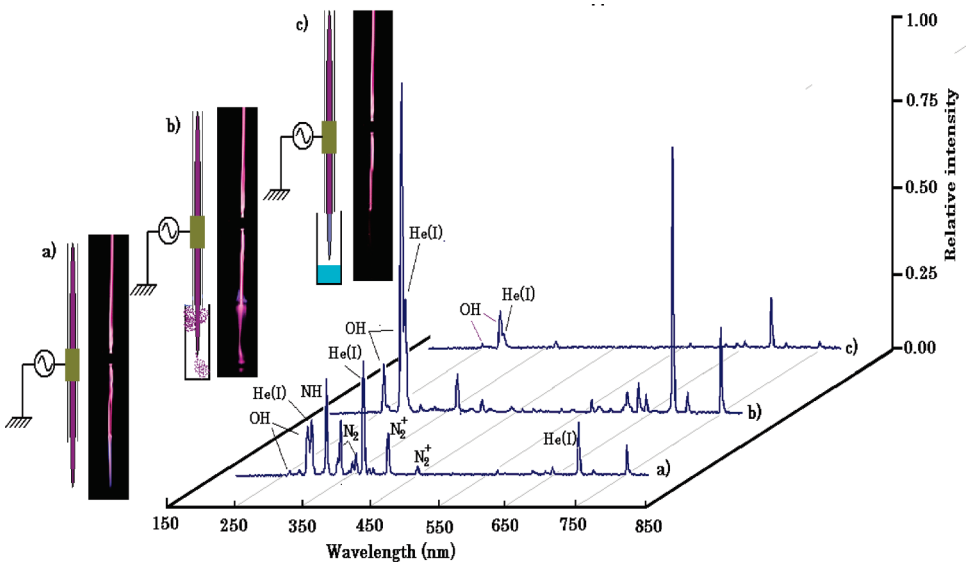

Figure 2. Emission spectra from DBD plasma jets emitted into (a) ambient air, (b) a quartz cell of 4.5 mL volume, and (c) a quartz cell of 4.5 mL volume that contains 1 mL of water. Schematic diagram of the DBD plasma-jet system (on the left side) and the corresponding photographs of DBD plasma jets (on the right side of the diagram in the dark background) in each case are also shown. Here the helium flow rate is 60 L/min and the peak voltage applied to the electrode is 8 kV with a frequency of 10 kHz.

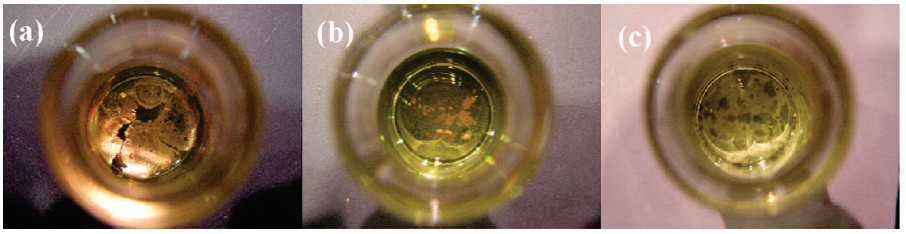

Figure 3. Formation of gold films and/or flakes on the surfaces of tetrachloroauric acid solutions by DBD plasma-jet irradiation to each solution for 60 min. The concentrations of tetrachloroauric acid are (a) 0.12 wt %, (b) 0.06 wt %, and (c) 0.012 wt %.

Naturally, the emission intensities of plasma-generated excited species depend on the applied voltage and gas flow rate. In our experiments, the emission intensities of all observed species were highest when the helium gas flow rate was in the range of 60 to 80 mL/min (see Figure S4 of the Supporting Information). When the helium gas flow rate was 60 L/min, the most intense emission lines were obtained when the applied peak voltage and frequency were 8 kV and 10 kHz. These discharge conditions were used in the experiments shown in the subsequent subsections.

3-2. Preparation and Analysis of the Gold Nanoparticles. *3-2-1. Plasma-Induced Reduction of Tetrachloroauric Acid.* To confirm the reduction reactivity by DVD plasma jets, we injected DBD helium plasma jets directly into tetrachloroauric acid solutions of various concentrations in the absence of any other reducing agents. Figure 3 shows photographs of the solution surfaces, upon which thin gold films and/or flakes were formed after DBD plasma-jet irradiation for 60 min. In the case of 0.12 wt % (a), a thin gold film with metallic luster was formed on the solution surface. The size of the gold film decreases with a decrease in the concentration of tetrachloroauric acid, as shown from parts (a) to (c) in Figure 3. Because no reducing agent was added to the tetrachloroauric acid solutions, some reactive species produced by the DBD plasma jets must have reduced aurate cations to elemental gold on the solution surface. On the basis of these observations, we conjectured that gold nanoparticles, rather than gold flakes, would be formed under similar experimental conditions in the presence of a suitable dispersant such as N6-PEG.

It is known that PEG−polyamine alone can reduce aurate cations (self-reduction) under acidic conditions.[7,42] When a solution of aurate cations containing N6-PEG was agitated at room temperature in an acidic media (pH 3.9), the color of the solution gradually became pinkish-red. The presence of gold nanoparticles in the medium was confirmed by the detection of a surface-plasmon band at 520 nm (Figure 4). This indicates that N6-PEG is self-reductive, as in the case of PEG-*b*-PAMA.[7,42]

We previously reported that coordination of PEG−amines onto a gold nanoparticle is much stronger in an alkaline environment because of coordination of a lone pair of a nitrogen atom to a gold surface.[44] However, under alkaline conditions, self-reduction between aurate cations and N6-PEG hardly occurs. From the experiments shown in Figure 3, one would expect that aurate cations may be reduced by DBD plasma-jet irradiation even under alkaline conditions.

Therefore, in both acidic and alkaline conditions (i.e., pH 3.9 and 10), we applied DBD plasma jets to tetrachloroauric acid solutions, with the tetrachloroauric acid/N6-PEG molar ratio being 1:5. Figure 5 shows the plasmon absorbance with and without DBD plasma-jet irradiation under pH 3.9 and 10 as a function of the reaction time, i.e., the period of DBD plasma-jet irradiation or that of self-reduction reactions. Under the acidic conditions (i.e., pH 3.9) given in Figure 5a, it is clearly shown that DBD plasma-jet irradiation accelerates the reducing reactions, as denoted by the solid circles. On the other hand, it is also shown that plasma-induced reduction proceeds and gold nanoparticles are formed even under alkaline conditions (i.e., pH 10) given in Figure 5b, which are denoted by the solid circles. In Figure 5a,b, solid squares represent absorption spectral data for self-reduction.

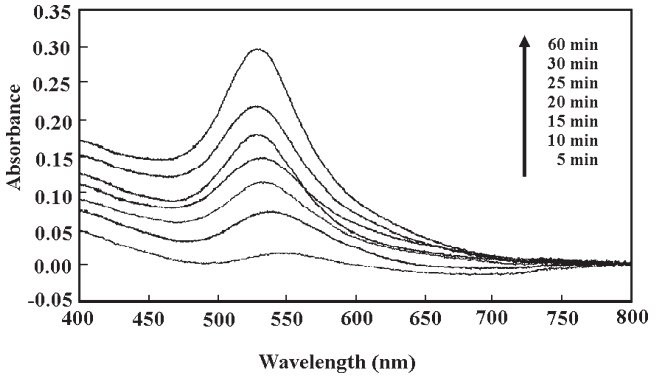

Figure 4. Time evolution of the surface-plasmon band for gold nanoparticles prepared by a N6-PEG self-reduction reaction under pH 3.9, with the P/A ratio being 5.

Figure 6 compares the size distributions of gold nanoparticles prepared with (a) and without (b) DBD plasma-jet irradiation under the acidic conditions of pH 3.9. The size distributions were obtained from DLS spectroscopy. In the case of plasma-induced reduction, a narrower size distribution of gold nanoparticles [with the second-order polydispersity index (SPDI) being 0.29] was obtained than that in the case of self-reduction (with SPDI being 0.5). SPDI represents the variance of the particle distribution, given by the value μ/Γ^2, with μ and Γ being known as the second cumulant and average decay rate of the first-order autocorrelation function obtained from the scattered light in DLS.[49]

To check whether DBD plasma jets can modify N6-PEG, we analyzed N6-PEG by SEC after DBD plasma-jet irradiation with different irradiation periods. Figure 7 shows SEC data for N6-PEG after various time durations (0, 30, 60, and 90 min) of DBD plasma-jet irradiation with a flow rate of 60 L/min, a discharge frequency of 10 kHz,

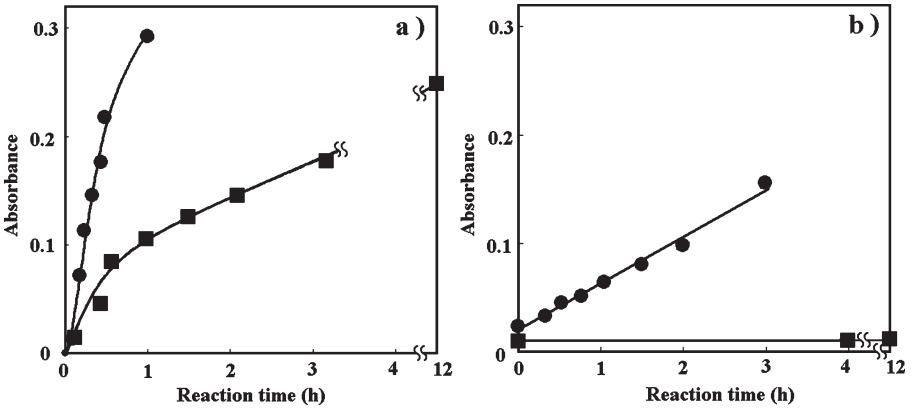

Figure 5. Time dependence of absorption spectra of the surface-plasmon band (520 nm) of gold nanoparticles prepared in the presence of N6-PEG with (denoted by solid circles) and without (denoted by solid squares) DBD plasma-jet irradiation. The P/A ratio was 5 and the concentration of aurate cations was 10^{-4} M in all cases. Here the solutions are (a) acidic (pH 3.9) and (b) alkaline (pH 10).

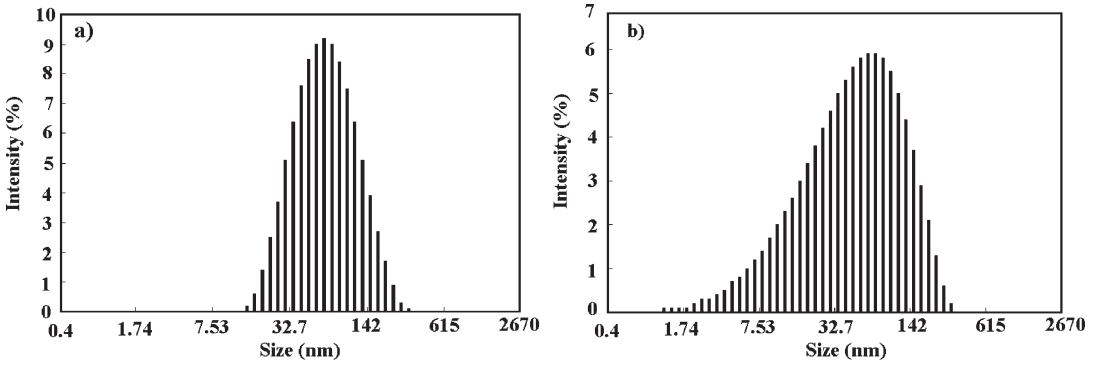

Figure 6. Particle size distributions of gold nanoparticles prepared with (a) and without (b) DBD plasma-jet irradiation. The solutions were maintained in acidic conditions (pH 3.9) and contain N6-PEG at a P/A ratio of 5. The peak and SPDI are 70 nm and 0.29 in part (a) and 62 nm and 0.50 in part (b). Clearly gold nanoparticles prepared by DBD plasma-jet irradiation have a narrower size distribution.

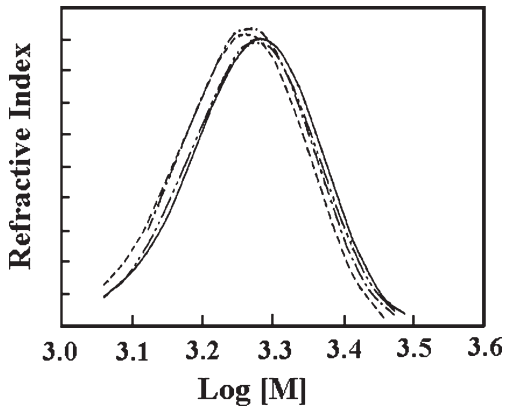

Figure 7. SEC data of N6-PEG solutions exposed to DBD plasma-jet irradiation for various time durations. The solid curve represents data for N6-PEG with no plasma irradiation (M_n = 1840), the dotted curve those for 30 min of irradiation (M_n = 1804), the dashed curve those for 60 min of irradiation (M_n = 1836), and the double-dashed curve those for 90 min of irradiation (M_n = 1759).

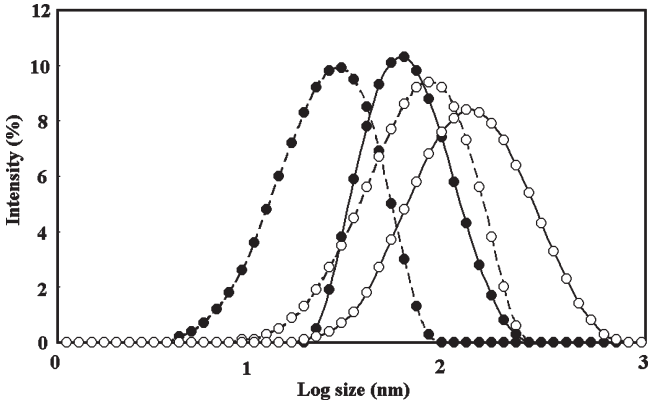

Figure 8. Size distributions of gold nanoparticles prepared by DBD plasma-jet irradiation for 90 min in the presence of N6-PEG under different P/A ratios and pH conditions. The P/A ratios are 10 (denoted by open circles) and 20 (denoted by closed circles), and the pH values are 3.9 (denoted by solid curves) and 10 (denoted by dotted curves).

and a peak voltage of 8 kV. As shown here, no essential change in the molecular mass was observed. These observations indicate that DBD plasma jets reduce aurate cations without affecting the essential characteristics of N6-PEG polymers.

Figure 8 shows the size distributions for gold nanoparticles prepared by DBD plasma-jet irradiation under different conditions, with the P/A ratio, which denotes the [N6-PEG]/[aurate cation] ratio, being 10 or 20 and the pH being 3.9 or 10. For gold nanoparticles prepared at pH 3.9 and a P/A ratio of 10, the average diameter was 142.2 nm and SPDI was 0.28, whereas those prepared at the same pH (3.9) and a P/A ratio of 20, the average diameter and SPDI were 58.5 nm and 0.22. As these experiments indicate, smaller gold nanoparticles with a narrow size distribution are obtained with higher concentrations of N6-PEG, owing to the prevention of gold nanoparticle coagulation by N6-PEG.

(49) Berne, B. J.; Pecora, R. Dynamic Light Scattering with Application to Chemistry, Biology, and Physics; Dover Publcations, Inc.: New York, 2000; pp 164−200.

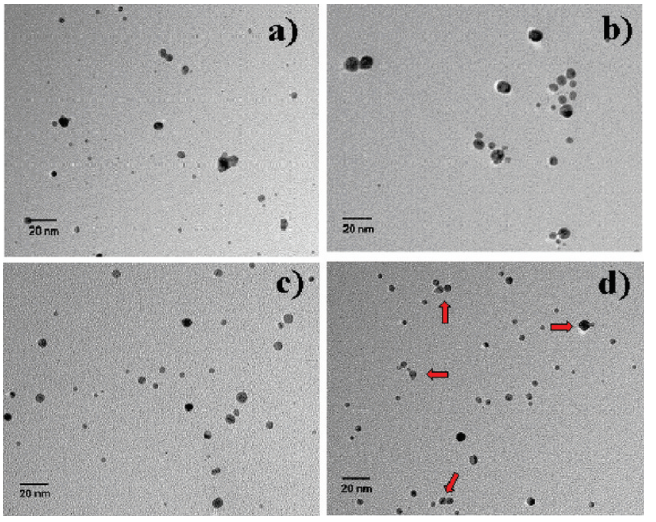

Figure 9. TEM images of gold nanoparticles prepared by DBD plasma-jet irradiation for 90 min under pH 3.9, with the P/A ratios being (a) 20 and (b) 10, and under pH 10, with the P/A ratios being (c) 20 and (d) 10. The arrows in part d indicate coagulated particles.

Under alkaline conditions (pH 10), even much smaller gold nanoparticles were obtained from plasma-induced reduction. When the P/A ratio was 10, the average diameter and SPDI of plasma-reduced gold nanoparticles were 77.3 nm and 0.26. With a further increase of the P/A to 20, these values became 26.7 nm and 0.28.

The morphologies of gold nanoparticles obtained by plasma-induced reduction were observed with TEM. When the P/A ratio was 5, the obtained nanoparticles were completely coagulated (see Figure S5 of the Supporting Information). The difference between the DLS data shown in Figure 6 and TEM data shown in Figure S5 of the Supporting Information is probably due to the sample preparation process. On the contrary, almost well-dispersed nanoparticles were obtained when gold nanoparticles prepared at pH 3.9 with P/A ratios of 20 and 10 were used, as shown in Figure 9a,b. In addition, the average particle size decreases remarkably with an increase in the P/A ratio. However, slight coagulation was still observed at a P/A ratio of 20 when the reaction was carried out under acidic conditions of pH 3.9. On the other hand, highly dispersed nanoparticles with narrow size distribution were obtained when the reaction was carried out under alkaline conditions of pH 10, as shown in Figure 9c,d. Especially, when the reaction was carried out at pH 10 with at a P/A ratio of 20, no remarkable coagulation was observed by TEM analysis, while slight coagulation was observed, as indicated by the arrows in Figure 9d, when the reaction was carried out at pH 10 with a P/A ratio of 10. We previously reported that deprotonated amines of PEG-*b*-PAMA bond to the surface of a gold nanoparticle by coordination.[44] From such studies, the formation of coordination bonds between N6-PEG and aurate cations is expected to occur.

From the experimental results given above, a higher P/A ratio under alkaline conditions is found to be more suitable for the preparation of gold nanoparticles with smaller sizes and a narrow size distribution. As mentioned

earlier, no reduction of tetrachloroauric acid occurs under alkaline conditions without DBD plasma-jet irradiation. In a tetrachloroauric acid solution under acidic conditions, gold atoms are known to be in the form of $AuCl_3(OH)^-$, which can be rapidly reduced by conventional reducing agents, such as ascorbic acid, disodium citrate, and sodium tetrahydroborate.[50,51] On the other hand, under alkaline conditions, gold atoms form $[AuCl_2(OH)_2]^-$ and/or $[AuCl(OH)_3]^-$, which can hardly be reduced by such conventional reducing agents. Therefore, DBD plasma-jet irradiation offers a unique way to reduce such aqua complexes under alkaline conditions without damaging N6-PEG polymers.

The N6-PEG-modified gold nanoparticles are expected to have long-term stability under physiological conditions. To confirm this, we purified the gold nanoparticles by centrifugation, which removes free N6-PEG from the solution, and changed the solvent of gold nanoparticles from a reaction mixture (pH 3.9 or 10) to a phosphate buffer (pH 7.4, 150 mM NaCl). The stabilities of such gold nanoparticles were evaluated by DLS and UV−vis spectrometry after they were kept in the phosphate buffer for 1 h at room temperature. When the gold particles were prepared under acidic conditions, i.e., pH 3.9, with the P/A ratio being 20 without plasma irradiation (self-reduction), the peak of the particle size distribution gradually shifts to a large value with an increase in the standing time and the average particle diameter shifts from 90.5 nm (at 1 h) to 259 nm (at 15 h) (Figure S6a of the Supporting Information). Clearly, the gold nanoparticles prepared by self-reduction under acidic conditions are unstable under physiological conditions. On the other hand, the gold nanoparticles prepared by DBD plasma-jet irradiation are more stable at least for 15 h. However, even plasma-reduced gold nanoparticles started to aggregate after 30 h under physiological conditions if they were prepared in acidic solutions. The average particle diameter and SPDI of plasma-reduced gold nanoparticles shifted from 66.0 nm and 0.211 (at 1 h) to 106.5 nm and 0.530 (at 30 h) (Figure S6b of the Supporting Information).

Figure 10 shows the time dependence of dispersion stabilities prepared at alkaline conditions (pH 10 with P/A ratios of 10 and 20). In contrast to gold nanoparticles prepared under acidic conditions, those prepared by plasma reduction under alkaline conditions are substantially more stable under physiological conditions. As shown in this figure, the size distribution of plasma-reduced gold nanoparticles prepared with a P/A ratio of 10 (represented by outline symbols), whose average diameter and SPDI were 68−77 nm and 0.26−0.27,

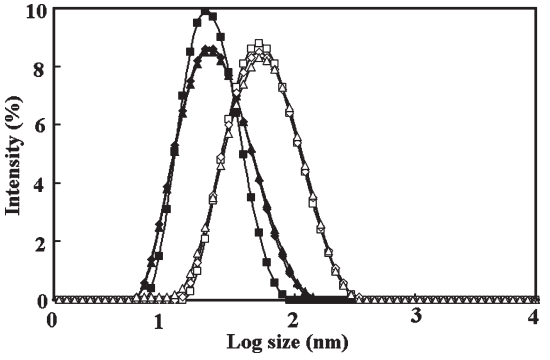

Figure 10. Dispersion stabilities under physiological conditions for gold nanoparticles prepared by different P/A ratios. All gold nanoparticles were prepared by plasma-induced reduction under alkaline conditions, i.e., pH 10. The solid symbols represent data for a P/A ratio of 20, and the outline symbols represent those for a P/A ratio of 10. The shapes of the symbols indicate different standing periods; the square, diamond, and triangle represent 1, 15, and 30 h, respectively.

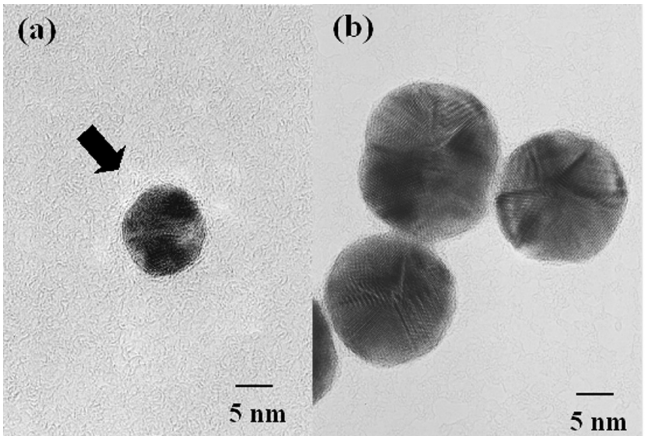

Figure 12. HRTEM images of (a) one of the purified gold nanoparticles prepared by DBD plasma-jet irradiation under pH 10, with the P/A ratio being 20, and (b) commercially available gold nanoparticles.

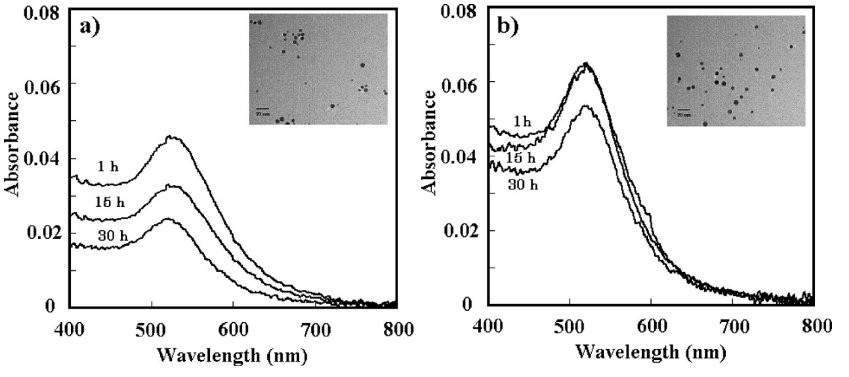

Figure 11. Time evolution of the surface-plasmon band for gold nanoparticles prepared under different conditions. In parts (a) and (b), the gold nanoparticles were prepared by DBD plasma-jet irradiation for 90 min under pH 10, with P/A ratios being 10 (a) and 20 (b). TEM images of gold nanoparticles after 30 h of standing at room temperature. In neither case is coagulation observed.

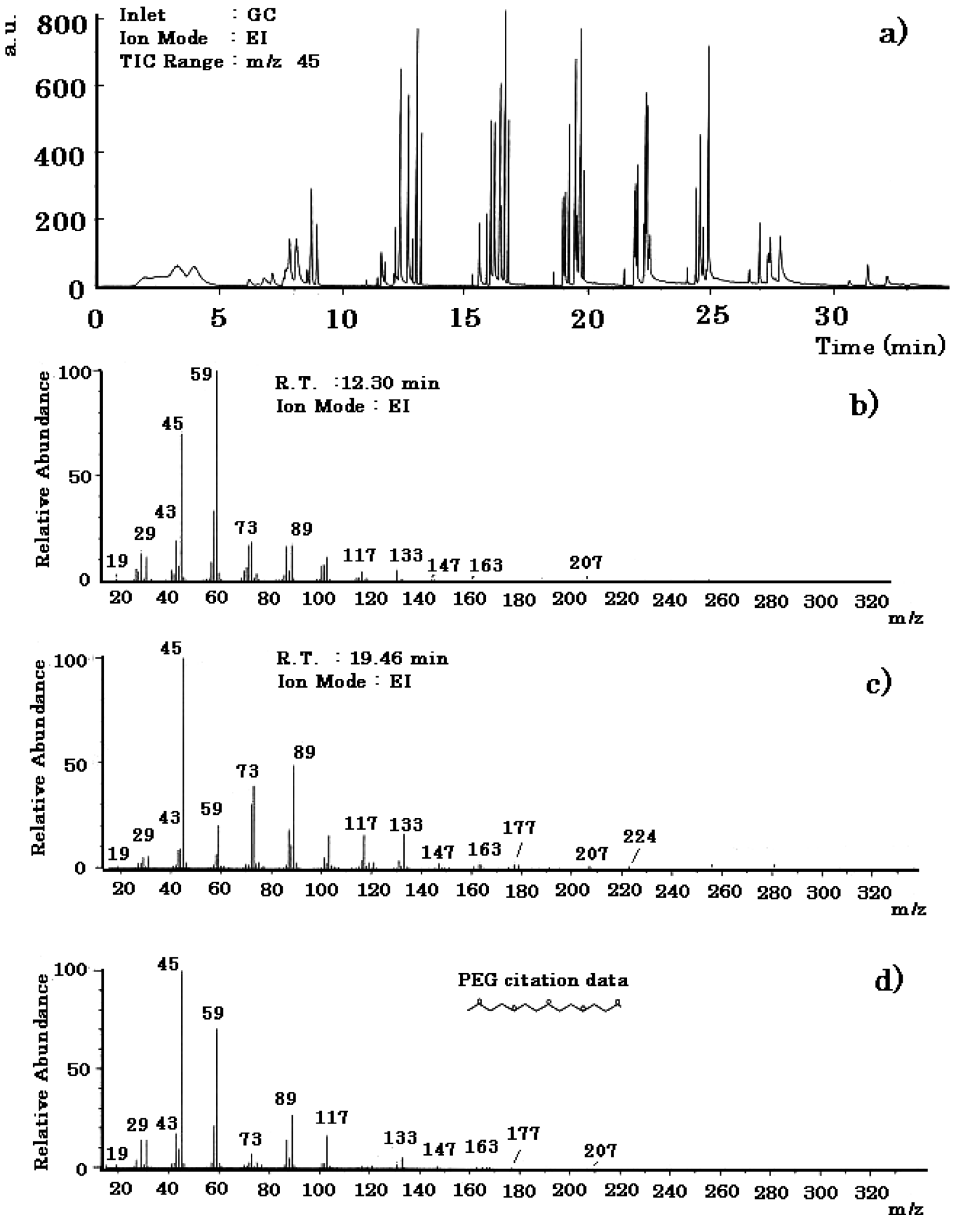

Figure 13. Data from pyrolysis GC−MS of purified gold nanoparticles prepared by DBD plasma-jet irradiation under pH 10, with the P/A ratio being 20. In part (a), mass chromatography of all fragments from pyrolysis of the N6-PEG-modified gold nanoparticles is shown. MS data for the N6-PEG-modified gold nanoparticles at retention times of 12.30 and 19.46 min are given in parts (b) and (c), respectively. The citation data (EPA/NIH Mass Spectral Data Base) of MS for PEG by pyrolysis GC−MS are given in part (d).

hardly changed for 30 h, although their average diameter was relatively large. On the other hand, gold nanoparticles similarly prepared with a P/A ratio of 20 (represented by solid symbols) have much smaller particle sizes and their size distribution also remained almost constant (with the average diameter and SPDI being 27−28 nm and 0.28−0.32) for 30 h.

In order to further assess the colloidal stability, we measured the surface-plasmon bands of gold nanoparticles produced with N6-PEG dispersant discussed above by a UV−vis spectrometer as a function of time. When the gold nanoparticles were prepared under acidic conditions (pH 3.9) with N6-PEG at a P/A ratio of 20, the surface-plasmon band at 520 nm decreased gradually with an increase in time and disappeared completely regardless of plasma irradiation (Figure S7 of the Supporting Information). In Figure 11a,b, the gold nanoparticles were prepared under alkaline conditions (pH 10) by plasma-reduced reduction with P/A ratios of 10 and 20, respectively. Corresponding TEM images of gold nanoparticles are given as insets in Figure 11. In Figure 11a, the surface-plasmon absorption continued to decrease for 30 h, although the peak position and half-bandwidth hardly changed, which indicates that no significant coagulation took place. Indeed, as shown in the TEM image in Figure 11a, coagulation of the nanoparticles was not observed after 30 h of standing at

(50) Ji, X.; Song, X.; Li, J.; Bai, Y.; Yang, W.; Peng, X. *J. Am. Chem. Soc.* **2007**, *129*, 13939–13948.
(51) Bhargava, S. K.; Booth, J. M.; Agrawal, S.; Coloe, P.; Kar, G. *Langmuir* **2005**, *21*, 5949–5956.

room temperature. Therefore, the decrease in the plasmon absorbance shown in Figure 11a may be attributed to the adhesion of gold nanoparticles to the vessel walls. On the other hand, in Figure 11b, the decrease in the plasmon absorption profile hardly changed for 30 h. The TEM image after 30 h of standing at room temperature given in the corresponding graph also indicates no coagulation.

In this way, it has been found that remarkably stable gold nanoparticles under physiological conditions can be prepared by plasma-induced reduction of aurate cations with N6-PEG at a P/A ratio of 20 and pH 10.

3-2-2. Structures of the Gold Nanoparticles. More detailed structures of gold nanoparticles can be observed by HRTEM. Figure 12 compares (a) a HRTEM image of gold nanoparticles prepared by plasma-induced reduction at pH 10 and a P/A ratio of 20 with (b) that of commercially available gold nanoparticles (British-Biocell International). Atomic structures of each nanoparticle core are clearly seen in both images. In Figure 12a, a white shadow is seen on the surface of the gold nanoparticle (indicated by arrows), which is likely a PEG layer. No such shadow is seen on the commercially available gold nanoparticles shown in Figure 12b.

We also performed energy-dispersed X-ray (EDX) microanalysis of gold nanoparticles prepared by plasma-induced reduction with N6-PEG. However, the EDX spectra (the data are not shown here) showed no trace of nitrogen and carbon, which can originate from N6-PEG of such particles. The PEG layers around gold nanoparticles may be too thin to be detected in EDX microanalysis.

To confirm the presence of such PEG layers, we purified the plasma-reduced gold nanoparticles (i.e., removed free N6-PEG from the solution) and analyzed them by pyrolysis GC−MS. The results are shown in Figure 13. The identification of each fragmentation was carried out by a comparison with the citation data in the EPA/NIH Mass Spectral Data Base.[52] Figure 13a shows the GC data for all pyrolyzed components from the gold nanoparticles prepared in the present study. Pyrolyzed components detected in the GC were analyzed by mass spectrometry. The mass fragmentations of the pyrolyzed compounds (with GC retention times being 12.30 and 15.46 min) are shown in parts (b) and (c) of Figure 13. Figure 13d shows the citation data for the mass fragment pattern of PEG. These mass fragmentation patterns are in close agreement with the citation data for PEG. Other pyrolyzed components showed similar results. Therefore, we conclude that PEG derivatives are present around the gold nanoparticles.

(52) Heller, S. R.; Milne, G. W. A. Library of Congress Cataloging in Publication Data, EPA/NIH mass spectral data base; U.S. Department of Commerce: Washington, DC, 1980; p4520.

4. Conclusions

In this study, we have presented a novel method for the preparation of gold nanoparticles from aurate cations using nonequilibrium atmospheric-pressure DBD plasma jets and N6-PEG. It has been shown that auric cations can be easily reduced by DBD plasma-jet irradiation to tetrachloroauric acid solutions of various concentrations and reduced cations form gold films and/or flakes on the solution surface in the absence of N6-PEG in the solution. In the presence of N6-PEG, on the other hand, small gold nanoparticles, rather than gold films or flakes, are formed because N6-PEG functions as a dispersant in the solution.

Reduction of auric acid can be done by N6-PEG only (which is known as self-reduction) under acidic conditions. However, DBD plasma-jet irradiation is found to be far more efficient in reducing auric cations under any pH conditions (including acidic and alkaline conditions). It has been confirmed by SEC that DBD plasma-jet irradiation does not degrade N6-PEG in the solution.

Because N6-PEG has been known to function as a dispersant much more effectively under alkaline conditions, gold nanoparticles formed under alkaline conditions by DBD plasma-jet irradiation with higher N6-PEG concentrations (e.g., with the P/A ratio being 20 at pH 10) have been found to exhibit excellent characteristics as nanoparticles, i.e., small sizes and narrow size distributions. Furthermore, gold nanoparticles prepared in this manner are found to have remarkable stability under physiological conditions because of the presence of N6-PEG-derived materials around the gold nanoparticles, which have been confirmed by both HRTEM and pyrolysis GC−MS. Such gold nanoparticles may therefore be considered excellent candidates for high-performance bionanoparticles.

Acknowledgment. This work was partially supported by a Grant-in-Aid for Scientific Research (A) (1800033) and World Premier International Research Center Initiative Program from the Ministry of Education, Culture, Sports, Science and Technology of Japan (MEXT).

Supporting Information Available: Synthetic route of N6-PEG, ^{1}H NMR of the tosylated PEG and N6-PEG, SEC and MALDI-TOF MS data of N6-PEG, optical emission spectra from DBD plasma jets, TEM images of a gold nanoparticle prepared by plasma reduction at pH 3.9 with a P/A ratio of 5, and the size distribution data and UV−vis spectra of a gold nanoparticle prepared with and without plasma irradiation at pH 3.9 with a P/A ratio of 20 (PDF). This material is available free of charge via the Internet at http://pubs.acs.org.